

Clustering Rate Analysis in Controlled Time-Scale Sensitometry

L. Dünkel*, E. Nutsch and B. Kutschan

Technische Fachhochschule Berlin, Fachbereich Mathematik/Physik, Rudower Chaussee 5, Geb. 10.2, D-12489 Berlin (Germany)

The paper presents a new methodology. Properly controlled sensitometry and analysis are used to unveil microscopic information from macroscopic response. The growth rate concept of the hierarchically coupled driving-force model (HCD-Model) provides an aggregated description that remains flexible enough to simulate sensitometric curves very precisely. By unique parameter identification and coherent interpretation, we obtain a simultaneous insight into interacting subsystems as determined by photoelectronic and ionic processes in combination with silver cluster nucleation and growth. Answers to substantial questions of AgX photophysics may be postponed largely to the end of the investigation if relevant results from quantitative analyses have been made available. The approach is outstanding for studies of latent image formation under realistic conditions such as moderate exposure and properly selected photomaterials.

Journal of Imaging Science and Technology 41: 521–530 (1997)

Introduction

AgX photophysics provides an important basis for any understanding of the photographic elementary process. But real-time studies during exposure are commonly bound to high-intensity sources that depart from normal imaging recording and may profoundly modify the system under investigation.¹ Accordingly, latent image theory suffers from serious shortcomings, as well. There are different hypotheses that have been discussed in detail for which molecular-scaled proof is not easy to supply.

With this in mind, we have engaged in developing a new methodology. Properly controlled time-scale sensitometry is used to reveal microscopic information from macroscopic response. But we are faced with an unclear situation. We need an aggregated description to reduce the number of unknown parameters that have to be identified. This must be provided by a coherent approach that remains flexible enough to simulate sensitometric curves very precisely.

Our model considers latent image formation as a photo-induced process of silver cluster nucleation and growth. We obtain a purely deterministic description called a hierarchically coupled driving-force model (HCD-Model). The fitting is carried out on sensitometric data that are correspondingly transformed to represent the time-dependent growth of a number of silver clusters of developable size. The transformations are in accordance with the previous assumptions of Nutting² and Silberstein.³ We identify the Burton–Berg corrected density⁴ with the average value of the fraction of developable silver halide grains by taking into account that one latent image center should be required, only, to develop a silver halide emulsion grain, completely.

This approach does not prefer any basic assumption that has been discussed controversially, so far. Relevant conclusions are postponed to the end of the investigation, if quantitative results have been made available from analy-

ses of realistic curves. The method corresponds to a top-down approach that differs substantially from both the models of Bayer and Hamilton⁵ and of Gerth.^{6–10} Simulations by these authors are bound strongly to very specified events according to a distinct concept of latent image theory. Little opportunity exists to revise them afterward in the context of final results. This article tries to give a self-contained account of the interrelated aspects published elsewhere in parts, up to now.^{11–17}

Systems Analysis Fundamentals

Formalism of the HCD-Model Approach. To simulate the photographic response, we use a differential equation system as given by

$$dx_1 / dt = A_1 - A_2 x_1 - A_3 x_1^2, \quad (1)$$

$$dx_2 / dt = B_1 x_1 + B_2 x_1^2 - B_3 x_1 x_2, \quad (2)$$

$$dx_3 / dt = C_1 x_1 (1 - x_3 / x_{2L})(x_2 - C_2 x_3), \quad (3)$$

$$dx_4 / dt = dx_3 / dt (1 - x_4 / K). \quad (4)$$

The model involves four variables assumed the most relevant for describing the process as considered here, i.e., the concentration of the photoliberated electrons in the conduction band, in the case of x_1 ; the total concentration of silver clusters photolytically formed during exposure, in the case of x_2 ; the concentration of silver clusters of developable size, in the case of x_3 ; and, the fraction of the developable silver halide emulsion grains, in the case of x_4 . All values are related to a distinct number of silver halide grains as designated by K in Eq. 4.

But to specify a realistic emulsion, many parameters are used as indicated by capital letters on the right side of the equation system. The parameters reflect different kinds of driving and retarding actions discussed more below.

Original manuscript received January 22nd, 1996.

* IS&T Member

© 1997, IS&T—The Society for Imaging Science and Technology

Correspondance with Statistical Rules. Our model deviates from the preference of statistics usually used for simulating the photographic response. According to Nutting,² time-independent chance distributions have been applied chiefly up to now.¹⁸ However, it does not seem very promising to combine growth rate equations with statistics for our purposes. We require a homogeneous description by one concept alone. Therefore, it seems very important to demonstrate that our formulation obeys statistical rules as well.

We refer to Eq. 4 which puts the growth rate for the number of developable grains $dx_4(t)/dt$ into a product of two factors, i.e., into $dx_3(t)/dt$ and into $[1 - x_4(t)/K]$, respectively. Thus, the rate of the developable grains is assumed proportional to the rate of development centers, as designated by $dx_3(t)/dt$. But the rate equation converges to zero if $x_4(t)$ approaches a distinct number of silver halide grains, as designated by K . This is due to the second factor that represents a logistics term.

The integration may be carried out by variable separation according to

$$x_4(t) = K(1 - e^{-x_3(t)/K}), \quad (5)$$

with the boundary conditions $x_4(t) = x_3(t) = 0$ for $t = 0$. Surprisingly, the result is completely identical with the famous Svedberg formula,¹⁹ established in 1922. In this case, a Poisson distribution function $P(n)$ is assumed to designate the probability for the occurrence of a grain with n development centers if the average number of development centers per grain amounts to \tilde{n} :

$$P(n) = \tilde{n}^n e^{-\tilde{n}} / n!. \quad (6)$$

The symbol \tilde{n} in Eq. 6 is identical to the exponential expression $x_3(t)/K$ in Eq. 5. From Eq. 6, we derive the fraction of grains with no development center according to

$$P(0) = e^{-\tilde{n}}. \quad (7)$$

The difference from unity designates the fraction of grains that involve one development center, at least. But this is the same result as expressed within the brackets on the right side of Eq. 5.

We consider the equivalence as the first proof of the relevance of our approach. The result is due to the influence of the retarding action, as expressed by the second factor above. It should be emphasized that retarding influences are very important for other levels of the model too.

Reference to the Lotka-Volterra Model. The Lotka-Volterra Model is well known for describing the dynamic balance between hares and foxes.²⁰ We speak of the predator-prey concept, in a more general sense. But our approach considers a similar situation. Four aggregated subsystems are designated by x_1 to x_4 , and we obtain some sort of growth rate coupling to provide interaction between them.

All levels are driven by a particular input value that corresponds to the photon absorption rate as designated by the driving-force parameter A_1 , in Eq. 1. This parameter must be adjusted to an average number K of silver halide grains as in Eq. 4. In this way, we obtain an analogy with the given "territory," as assumed for defining the occupation densities in the predator-prey concept. But in

comparison with the latter, we may profit from substantial simplifications as summarized in the following:

1. Rate coupling occurs in a unidirectional way only. In other words, no feedback occurs between subsequent levels in a reciprocal way, as designated by the rate equations for the four variables x_1 to x_4 , respectively.
2. Nonlinearity, as originally introduced by mixed expressions of different variables like x_1x_2 or x_1x_3 , is finally reduced, owing to the substitution of the variable x_1 by the constant limit value x_{1L} , as outlined below.

References to AgX Photophysics

Use of the Tichonov Theorem. With respect to further application, we present the model in the integral form*:

$$x_4 = K(D_{\text{absolut}} - Fog) / (D_{\text{max}} - Fog), \quad (8)$$

$$x_3 = -K \ln(1 - x_4 / K), \quad (9)$$

$$x_2 = x_{2L} \left(1 - e^{-x_{1L}t}\right), \quad x_2 = 0 \text{ if } t = 0, \quad B_3 = 1, \quad (10)$$

$$x_{1L} = -A_2 / 2A_3 + \left(A_2^2 / 4A_3^2 + A_1 / A_3\right)^{1/2} \text{ if } A_3 \neq 0, \quad (11)$$

$$x_{1L} = A_1 / A_2 \text{ if } A_3 = 0 \text{ if } A_2 \neq 0. \quad (12)$$

Burton-Berg corrected densities are transformed according to both Eqs. 8 and 9 to obtain the growth of the number of developable grains, as derived from time-scale sensitivity. All subsequent equations contain the limit value x_{1L} instead of the variable x_1 . The reason is demonstrated by corresponding simulations as performed with our model in Fig. 1.

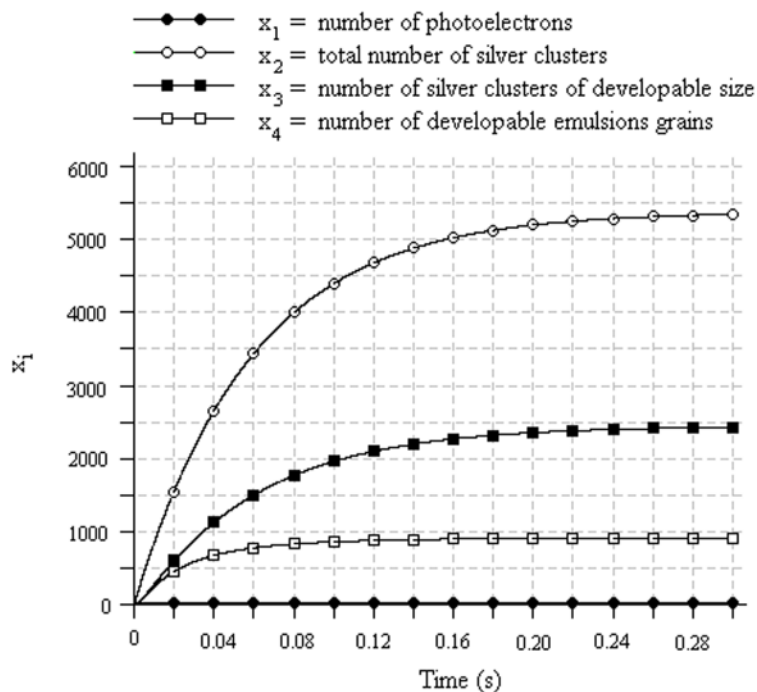
The variable x_1 reaches a steady-state value in a very short time (on the order of microseconds), whereas changes of the other variables take longer (on the order of milliseconds and more). Because of the great difference between the time constants, we obtain no dynamic interference between photoelectron excitation and the other processes connected with silver cluster nucleation and growth. Such a situation corresponds to the Tichonov theorem[†] as established in 1952.²¹ Therefore, we may approximate the variable of the process with the shortest time constant by the constant limit value of the steady state as derived from the photostationary condition $dx_1/dt = 0$ in Eq. 1.

But in Eq. 10, a second limit value x_{2L} appears. The expression has been obtained by direct integration of Eq. 2, considering the Tichonov theorem as mentioned before. From the stationary condition $dx_2/dt = 0$, we may derive

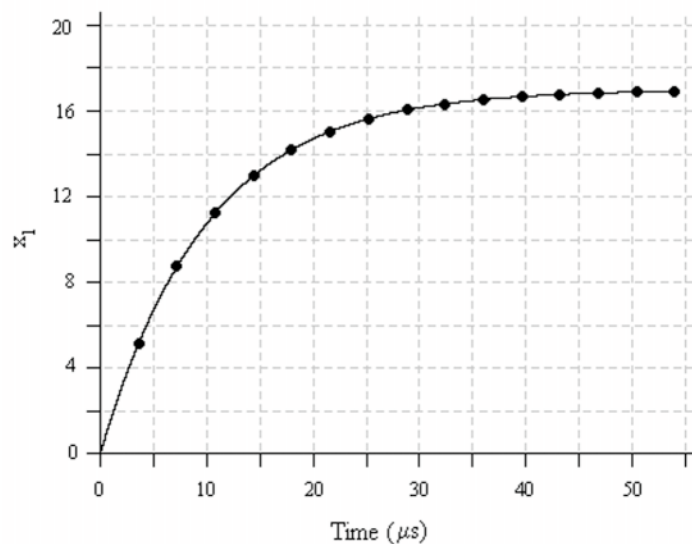
$$x_{2L} = B_1 + B_2x_{1L} \quad \text{for} \quad B_3 = 1. \quad (13)$$

* The factor K is introduced for customary reasons in accordance with previous publications where the corresponding value has been assumed always arbitrarily as $K = 1000$. The consideration of a multitude of emulsion grains seems more convenient, in our opinion, than the restriction to one grain alone. Furthermore, we have the opportunity for a reasonable calibration in this way, which may provide more convenient orders of magnitude for the parameters to be identified.

† The term is well known in systems analysis,²⁷ because Tichonov was the first to give a strong definition from a mathematical point of view. In today's physics and natural sciences, however, equivalent formulations are used preferably, as termed as *slaving principle* or *adiabatic deviation*.²⁸



$$\begin{aligned}
 A_1 &= 1.7 \cdot 10^6 \text{ s}^{-1} \\
 A_2 &= 1.0 \cdot 10^5 \text{ s}^{-1} \\
 A_3 &= 0 \text{ s}^{-1} \\
 B_1 &= 4.0 \cdot 10^3 \text{ s}^{-1} \\
 B_2 &= 8.1 \cdot 10^1 \text{ s}^{-1} \\
 C_1 &= 9.0 \text{ s}^{-1} \\
 C_2 &= 2.2 \text{ *)} \\
 K &= 1000
 \end{aligned}$$



$$\begin{aligned}
 x_{1L} &= 17 \\
 x_{2L} &= 5383 \\
 x_{3L} &= 2422
 \end{aligned}$$

Figure 1. Demonstration of the Tichonov theorem. The growth curve simulations with the HCD-Model are in accord with the results of the analysis of a diagnostic x-ray film as presented in Fig. 2. The photo steady-state for the variable x_1 is reached well before silver cluster nucleation and growth become remarkable. The asterisk by the parameter C_2 is a note that according to the rate Eq. 3, the parameter C_2 must be dimensionless if the corresponding dimension (s^{-1}) is assigned to the parameter C_1 .

The discussion of this last result will be postponed to the relevant section below.

Grain Size Influence. This influence is correlated with the photon absorption rate as obtained for a distinct number of emulsion grains. We obtain a direct dependence on the average size of the emulsion grains. The greater the emulsion grain the greater the photon absorption rate per grain, and the greater the speed of all other processes as mediated by the limit value x_{1L} , according to Eq. 12, for example.

But another aspect is worthy of mention. Both parameters A_1 and K are unique and have to be determined by

direct measurement independently of any fitting at sensitometric curves. Thus, a well-equipped sensitometer with proper radiometry is required to obtain the absolute number of photons to be absorbed per unit time and unit area. This must be supplemented by microscopy and related methods to characterize the grain size and density within the photographic layer.

Photoelectron Excitation Process. This process is understood quite controversially by different concepts of current latent image theory. According to Gurney and Mott, a pair generation of free electrons and holes is assumed. But Mitchell¹ discusses an Auger decay of excitons at so-called

donor centers that excludes the generation of holes in the usual case.

In Eq. 1, however, such a distinction does not play a primary role. Photoexcitation of free electrons is thought to depend directly on the photon absorption rate as expressed by A_1 . In addition, two loss processes of different kinetic order are assumed for photoelectron trapping at isolated states and for band-to-band recombination with holes. The corresponding terms are designated by both parameters A_2 and A_3 , respectively. This is a standard formulation as usually applied to describe photoexcitation in semiconductor systems.²²

By identifying the limit value x_{1L} , we get the photoelectron lifetime τ according to

$$\tau = x_{1L}/A_1. \quad (14)$$

This is one of the most important quantities we derive with the help of our model. The reversal of τ yields the trapping parameter A_2 , provided that the recombination parameter A_3 may be assumed as zero. Accordingly we obtain

$$\tau = 1/A_2. \quad (15)$$

The validity of Eq. 15 has been proven in many studies where a linear relationship has been found between both quantities x_{1L} and A_1 .

Silver Cluster Nucleation Process. Silver cluster nucleation involves an initial stage leading to subimage formation. The clusters are still smaller than the size necessary for initiating development. But they may act as concentration centers to gather photoelectrons and mobile silver ions at the same site by further exposure.

In the approach in Eq. 2, no distinct specification has been made whether the subimages should be assumed as Ag_2 aggregates or as Ag_1^+ concentration centers according to direct photolysis or to the photoaggregation theory, respectively.¹

By considering the Tichonov theorem, we get a more concise description for both the differential and integral form, as given by

$$dx_2/dt = x_{1L}(x_{2L} - x_2) \quad (16)$$

and

$$x_2 = x_{2L}(1 - e^{-x_1 t})$$

referring to Eq. 10. In this way, silver cluster nucleation should be described uniquely by both limit values x_{1L} and x_{2L} . But the latter are not constant quantities if the photon absorption rate is varied.

According to Eq. 2, we get two driving terms that designate first- and second-order processes depending on the photoelectron density. The parameters are B_1 and B_2 , respectively. The former process may be assigned to a step-by-step mechanism via photoelectron capture at deep traps. The latter considers higher ordered condensation as assumed by the thermodynamic phase-building concept,²³ for example.

But Eq. 2 involves yet a third term with a negative sign. We obtain a mixed expression as designated by $B_3 x_{1L} x_2$. The retardation should be due to different reasons that will not be explained in detail, i.e., restricted number of sensitivity centers, competition effects, thermal decay, etc.. Therefore, Eq. 2 reaches a limit value by extended exposure too.

Now, we refer to a special assumption made in Eq. 13 by setting $B_3 = 1$. With explicit consideration of B_3 we obtain a relevant formulation instead of Eq. 13 according to

$$x_{2L} = B_1/B_3 + (B_2/B_3)x_{1L}. \quad (17)$$

Equation 17 turns out to be overestimated. It is impossible to identify all three parameters independently. Similarly, we may derive a complete formulation for Eq. 10 with explicit inclusion of B_3 , as given by

$$x_2 = x_{2L}(1 - e^{-B_3 x_{1L} t}). \quad (18)$$

A product of two unknown quantities enters the exponential term, i.e., the retarding parameter B_3 and the limit value x_{1L} . Neither can be determined individually. Therefore, we need some supplementary arguments to justify the assumption above.

1. The main support is provided by the photoelectronic lifetime determination as derived from Eq. 14. In this way, a relevant order of magnitude could be revealed by all our studies to lie in the microsecond range.¹³
2. We restrict the consideration to very low values of x_{1L} where deep traps should be efficient only and where the higher order driving term may be neglected. Accordingly, we get two types of concentration centers solely, i.e., the sensitivity centers as connected with B_1 and the subimage centers as expressed by x_2 . Provided the efficiency of electron capture is the same, the reaction rate constant must be the same as well. This will correspond to the parameter B_3 , in both cases. By designating the number of sensitivity centers with B_1^* , we derive from Eq. 2 two expressions as given by

$$B_1 = B_3 B_1^* \quad (19)$$

and

$$dx_2/dt = B_3 x_{1L}(B_1^* - x_2). \quad (20)$$

Thus, x_2 converges to the number of sensitivity centers, exactly, if the limit value x_{1L} is very low. But as for the identification of B_3 , we have to refer to the same arguments as stressed in No. 1 above.

3. The parameter B_3 may be assumed to have a constant quantity in contrast to the limit value x_{1L} . Thus, corresponding changes of the unresolved product $B_3 x_{1L}$ may be interpreted properly as changes in x_{1L} . We are speaking of an *efficient* photoelectron density, therefore, if the identification of x_{1L} refers to the unresolved product above.

Silver Clustering Growth. As stated before, subimages need further exposure to reach a critical size. The growth rate is given by Eq. 3. By considering the Tichonov theorem, we obtain two major terms with a positive and a negative sign as expressed by $C_1 x_{1L} x_2$ and by $C_1 C_2 x_{1L} x_3$, respectively. Thus, the driving action is assumed dependent on the actual value of x_2 , whereas retardation appears as feedback in dependence on the actual value of x_3 . The direct influence of the first level of photoexcitation is mediated by the limit value x_{1L} .

But in addition, we must consider a second factor as given by $(1 - x_3/x_{2L})$. Its influence provides greater flexibility to

analyze experimental curves over the global range. We obtain an additional action that prevents in any case the variable x_3 from becoming greater than the limit value x_{2L} . We believe this should be consistent with a more adequate simulation as well, because retardations from differential origins would be considered more properly in this way. Unfortunately, the formulation becomes more complicated too. We obtain a Riccati differential equation discussed next.

Parameter Identification

Basic Problem. This problem is the most delicate one with which we are faced. The number of unknown parameters remains disproportionately large, despite all approximations as made so far, and no possibility exists for any direct identification in some analytical way. We have to refer to an indirect access by more expensive calculations to compare experimental with calculated data.

Below we consider the mathematical background more thoroughly. A crucial step is the integration of the Riccati differential equation. This is required to fit correspondingly transformed data that represent the time-dependent growth of the variable x_3 . The values for the variable x_3 are available from monochromatic time-scale sensitometry by transformations with the help of Eqs. 8 and 9, respectively.

Riccati Differential Equation. Starting from our model, we obtain this equation by a sequence of several steps. A summary should provide some help to follow further arguments.

1. We start with the model as originally given by Eqs. 1 through 4.
2. Under adequate consideration of the Tichonov theorem, the dynamic variable x_1 is replaced by the constant limit value x_{1L} according to the saturation condition $dx_1/dt = 0$ to be applied to Eq. 1.
3. With the substitution above, the integration of Eq. 2 is performed by variable separation in an analytically closed form to get Eq. 10. If not noted otherwise, we make use of the boundary condition as designated in Eq. 10. This means the retardation parameter is adjusted arbitrarily to the value of $B_3 = 1$.
4. In Eq. 10 a second limit value has to be considered that is designated by x_{2L} . In a similar way as above, the constant value resulting from the saturation condition $dx_2/dt = 0$ will be given by Eq. 13.
5. A substitution is carried out in Eq. 3 with respect to the dynamic variable x_2 , i.e., the variable on the right side of Eq. 3 is replaced by the integral function as provided by Eq. 10. In this way, Eq. 3 will be transformed into

$$dx_3 / dt = C_1 x_{1L} (1 - x_3 / x_{2L}) [x_{2L} (1 - e^{-x_{1L}t}) - C_2 x_3] \quad (20)$$

Multiplication of the right side in Eq. 20 and rearrangement lead to an expression:

$$y' + [a_3 (1 - e^{-a_1 t}) + a_4] y - (a_4 / a_2) y^2 - a_2 a_3 (1 - e^{-a_1 t}) = 0, \quad (21)$$

with $y' = dx_3/dt$, $y = x_3$, $a_1 = x_{1L}$, $a_2 = x_{2L}$, $a_3 = x_{1L}C_1$, $a_4 = x_{1L}C_1C_2$.

Eq. 21 exhibits an inhomogeneous differential equation of first order as indicated by three terms, i.e., by the dif-

ferential term involving the first derivative y' , by the linear term depending on y , and by the inhomogeneous term that does not depend on y , respectively. But in addition, there is a nonlinear term depending on the square of the integral function y , i.e., on y^2 . This is a special type of nonlinear differential equation, namely the Riccati differential equation, as mentioned before.²⁴

The renaming in Eq. 21 avoids unwieldy expressions as designated by a_3 and a_4 , respectively. But the renaming has been applied to both limit values x_{1L} and x_{2L} , too. This may seem unnecessary and quite confusing, because the physical meaning should be clearly expressed. However, proper standardization by four similar symbols facilitate further calculations requiring increasingly complex formulas.

Solution by a Polynomial Approach. The method is based on the linear independence between terms of differential polynomial order, because direct integration of the Riccati differential equation is too complicated to provide any successful approach.²⁴ By the calculations below, we obtain some supplementary information about the process itself. Straightforward application of the calculations may help consolidate parameter identification if not completely, in parts at least.

Thus, we substitute all time-dependent functions in Eq. 21 by a corresponding polynomial series as established according to

$$y(t) = b_0 + b_1 t + b_2 t^2 + b_3 t^3 + b_4 t^4 + b_5 t^5, \dots, \quad (22)$$

$$y'(t) = b_1 + 2b_2 t + 3b_3 t^2 + 4b_4 t^3 + 5b_5 t^4, \dots, \quad (23)$$

$$(1 - e^{-a_1 t}) = a_1 t + a_1^2 t^2 / 2! + a_1^3 t^3 / 3! - a_1^4 t^4 / 4! + \dots, \quad (24)$$

The polynomial series in Eq. 22 is assumed to be a general result for the integral function for which we have to search. Equation 23 is the first derivative of Eq. 22. Equation 24 is used to substitute exponential functions as involved in Eq. 27. The right side represents the Taylor series approximation leading to an alternating sign between subsequent terms of rising order.²⁵

In the final step, we obtain a set of equations for each power of t by considering the rule of linear independence that defines the conditions for the polynomial coefficients as assumed by Eq. 22. But the procedure involves continued multiplications between polynomial series as substituted in Eq. 21. Fortunately, we do not have to calculate ad infinitum. The important result is a recursive scheme summarized next.

1. Both first terms are missing on the right side of the polynomial approach as given by Eq. 22. Accordingly, we obtain

$$b_0 = b_1 = 0. \quad (25)$$

The proof will not be demonstrated in detail. But if we assume the clustering rate is zero for $t = 0$, the result in Eq. 25 appears correct because both Eqs. 22 and 23 must converge then to zero as well.

2. Accordingly, the coefficient b_2 is the first to play an efficient role. From our procedure, we obtain

$$b_2 = (1/2) a_1 a_2 a_3. \quad (26)$$

The result does not involve any retarding influence connected with the parameter a_4 . In the beginning, we obtain a concentrated charge that combines all relevant driving influences from different levels as expressed by the product above.

3. The subsequent coefficient is derived as

$$b_3 = (1/3) \left[(1/2) a_1^2 a_2 a_3 + a_4 b_2 \right]. \quad (27)$$

Returning to Eq. 26, we obtain a negative sign. An additional feature is the involvement of a_4 . Some indication of a recursive scheme is already evident. To calculate the coefficient b_3 , we must determine the coefficient b_2 first. But this aspect will concern us in more detail next.

4. For simplicity we will differentiate now between the situations of whether we analyze the beginning or the global range of the curve.

In the first case, we may neglect the logistics factor as involved in Eq. 20, i.e., the factor $(1 - x_3/x_{2L})$. Consequently, we obtain a proportionally simple expression to determine the polynomial coefficients for all indices n greater than 2 with a recursive formula:

$$b_n = (-1)^n (1/n) \left[1/(n-1)! a_1^{n-1} a_2 a_3 + (-1)^{n-1} a_4 b_{n-1} \right]. \quad (28)$$

It is easy to prove that Eq. 28 corresponds to Eq. 27 for $n = 3$.

5. The second case of the complete Riccati differential equation leads to a recursive formula as well. But we obtain a more sophisticated expression as given by

$$b_n = (-1)^n (1/n) \left\{ \left[2/(n-1)! a_1^{n-2} b_2 + a_4 b_{n-1} \right] - (1/n) a_3 \left[\sum_{i=1}^{n-3} (-1)^{i+1} (1/i!) a_1^i b_{n-1-i} \right] \dots - (a_4/a_2) \left(\sum_{i=2}^{n-3} b_{n-1-i} b_i \right) \right\}. \quad (29)$$

The last formula will be valid for $n \geq 4$, whereas the coefficients with smaller indices are described as above, i.e., by Eqs. 25 through 27.

It is out of our scope now to undertake each mathematical exercise to prove the strong validity of the recursive formulas by complete induction. The important question we are concerned with next may be formulated as follows. What can we sift out to consolidate parameter identification properly?

Methodology of Parameter Fitting and Identification. It seems advantageous to restrict the analysis to the beginning of the curve. All relevant information is included, and quite simplified equations may be used. However, this way is not very promising in reality. Data scatter becomes too great, and the unknown truncation error of the polynomial approach may not be well observed.

We present a compromise. We use numerical integration for fitting the global range. But the basic equation is modified by considering some specified solutions obtained before. The methodology is outlined as follows:

1. For the analysis of the beginning range, three polynomial coefficients are required to identify the parameters involved in Eq. 21. This means all parameters may be determined with the help of both Eqs. 26 and 28 if the values for the first three polynomial coefficients are known, i.e., the values for b_2 to b_4 . The correspondingly transformed equations are given elsewhere¹³ and will not concern us here in detail.

But in the context above we emphasize that we obtain a product $a_2 a_3$ only. Neither of the two parameters may be determined individually unless we use supplementary assumptions that will help us to solve this problem too.²³

2. For identifying the polynomial coefficients, computer programs are available that rely on function minimization.¹³ According to our experience, however, the correct determination of the coefficient b_4 appears seriously compromised. This is owing to the truncation error of the polynomial approach that may not be well observed.

Below we present alternative access that seems interesting from both a theoretical and a practical point of view. By considering Eq. 25, we may subdivide Eq. 22 by the squared exposure time t^2 according to

$$y(t)/t^2 = b_2 + b_3 t + b_4 t^2 + b_5 t^3 + b_6 t^4 \dots \quad (30)$$

Because the values on the left side of Eq. 30 are available from sensitometric data, proper extrapolation should reveal the first polynomial coefficient b_2 :

$$\lim_{t \rightarrow 0} y(t)/t^2 = b_2. \quad (31)$$

To identify both the coefficients b_3 and b_4 , we use a recursive procedure as given by

$$\lim_{t \rightarrow 0} [y_2(t) - b_2]/t = b_3 \quad \text{with} \quad y_2(t) = y(t)/t^2 \quad (32)$$

and

$$\lim_{t \rightarrow 0} [y_3(t) - b_3]/t = b_4 \quad \text{with} \quad y_3(t) = y_2(t)/t^2 - b_2/t. \quad (33)$$

The approach could be applied successfully in the case of undisturbed data as obtained from simulated results. In the case of empirical data, however, the scatter is too large for a straightforward identification using Eq. 33.

3. For fitting by numerical integration, we rewrite the Riccati differential equation:

$$dy/dt = (1 - y/a_2) \left[(2 \cdot b_2/a_1) (1 - e^{-a_1 t}) - a_4 y \right]. \quad (34)$$

Equation 34 corresponds to Eq. 20. As introduced by Eq. 21, the parameters a_1 and a_2 are identical with both limit values x_{1L} and x_{2L} . But in addition, there appears the coefficient b_2 that has been involved by considering the result of the polynomial approach as given in Eq. 26. Detailed explanation is given below.

4. In the fitting process, we have to adjust three quantities, mainly, i.e., b_2 , a_1 , and a_4 . As for the fourth parameter a_2 , no significant influence occurs on the

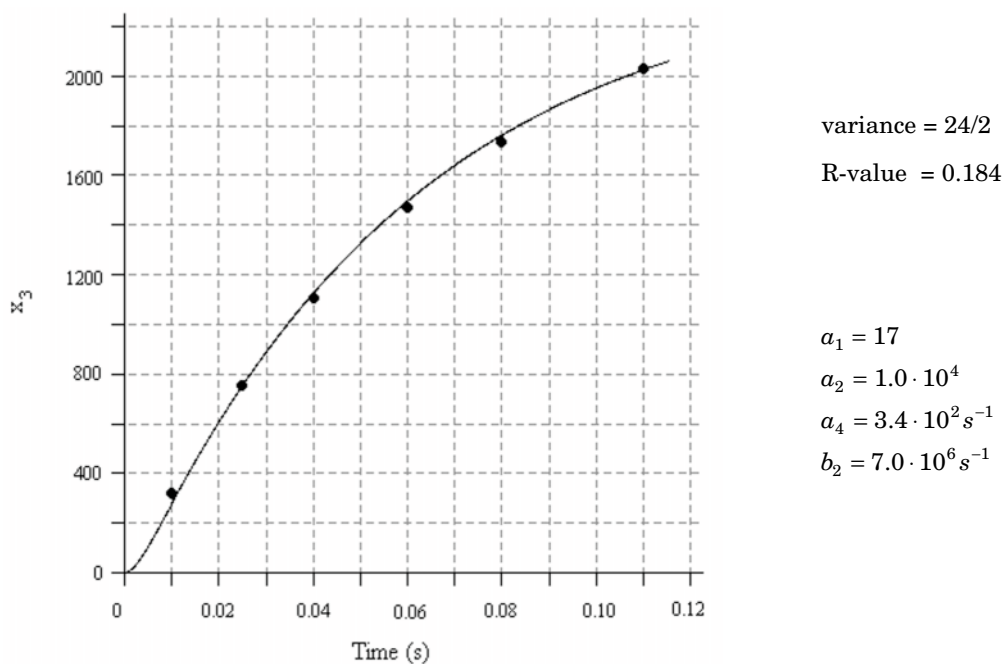


Figure 2. Example for fitting and analysis of correspondingly transformed data as obtained by monochromatic time-scale sensitometry with orthochromatic x-ray film T-TX-MFO (Typon AG, Switzerland) The absolute value of the photon absorption rate has been determined as 1.7×10^6 photons/s and $K = 1000$ emulsion grains for irradiation at 425 nm.

bending of the curve provided its value is assumed to be proportionally large. For better insight into the interaction between these quantities, we consider Eq. 35 as given by

$$dy / dt = (1 - y / a_2) \left[2 \cdot b_2(t - a_1 t^2 / 2 + a_1^2 t^3 / 3! - a_1^3 t^4 / 4! \dots) - a_4 y \right]. \quad (35)$$

Equation 35 has been derived from Eq. 34 by using the Taylor series approximation instead of the exponential term. We recognize the only driving action as assigned to the complex coefficient b_2 while both parameters a_1 and a_4 are bound to retarding actions.

5. By considering the above results, we may subdivide the fitting into two different steps:

The first involves the identification of the polynomial coefficient b_2 . Thereby, we may profit from its driving influence. This allows an approximate adjustment in the beginning of the curve. But other methods may be applied too, i.e., function minimization of the polynomial approach or corresponding extrapolation with the help of Eq. 31.

The second step refers to the simultaneous identification of both parameters a_1 and a_4 . This procedure is more delicate, because of the reversal influence of both values on each another. But as we have found, each of the parameters influences the global bending in some specific way. Thus, sufficiently unique identification is possible if the fitting is performed very carefully.

6. But regardless of whether the adjustment is performed by operator scan or automatically, in each case proper discrepancy factors are required to optimize the fit. Given a number m of data provided from time-scale

sensitometry, two discrepancy factors have been used as follows:

The variance as given by

$$V = \left\{ (1/m) \sum_{j=1}^m [y_j - y(t_j)]^2 \right\}^{1/2}, \quad (36)$$

and the R value is given by

$$R = \sum_{j=1}^m [y_j - y(t_j)] / y_j. \quad (37)$$

Analysis by Computer Dialog. An example is demonstrated in Fig. 2. The graph depicts the time-dependent growth of the variable x_3 , with $K = 1000$ emulsion grains. We get a well optimized fit between sensitometric data and simulated results. The photomaterial was orthochromatic x-ray film T-TX-MFO from Typon AG, Switzerland. Time-scale exposure has been carried out with monochromatic irradiation at 425 nm. (For further details see Ref. 17).

The corresponding discrepancy factors are given at the top right side of the graph. The column indicates the three quantities that have been systematically varied, i.e., b_2 , a_1 , and a_4 , respectively. The limit value a_2 is an approximated result and does not influence seriously the fitting process. The photon absorption rate was 1.7×10^6 /s and with $K = 1000$ grains. This should correspond to a photo-electronic lifetime of $\tau = 1.0 \times 10^{-5}$ s, according to Eq. 14.

An instructive result is the limit value x_{3L} . The corresponding saturation condition in Eq. 3 leads to an expression:

$$\begin{aligned} x_{3L} &= (2b_2) / (a_1 a_4) = \\ &= [2(a_1 a_2 a_3 / 2)] / (a_1 a_4) = \\ &= (a_2 a_3) / a_4 = x_{2L} / C_2. \end{aligned} \quad (38)$$

With our results, we obtain $x_{3L} = 2422$. Accordingly, about two and a half latent image centers should be formed on average per emulsion grain by extended exposure with the photon absorption rate as indicated above.

Outlines of Systematic Research

What Does the Exercise of Fitting Tell Us? The consolidation of parameter identification is a very important step for getting straightforward information in further research. But a coherent interpretation has to be secured as well. Below we consider two major lines that are interrelated in a substantial way, i.e., the analysis and aggregation of the response curve to obtain a photophysically well-specified insight into more detailed aspects and the proper combination of the results in context with systematic studies of more or less expressed effects in photographic behavior, e.g., low-intensity reciprocity law failure (LIRF), development influence, spectral dependence, influence of temperature, and double exposure effects. The interpretation of the first line is summarized as follows:

1. At the most aggregated level, we get the time-dependent growth curve of the variable x_3 . The result is assumed to reflect the actual number of latent image centers to be photolytically formed. From our model, we may derive a unique turning point once corresponding parameters have been identified. This point may be used to calculate a specified value that characterizes the maximum spectral quantum sensitivity for the photon absorption rate A_1 to be applied, i.e., by determining the minimum number of absorbed photons needed to form a single latent image center.
2. A primary result of the fitting process is the polynomial coefficient b_2 . But for further interpretation, we may not use this value alone, because of the unspecified combination of different driving forces, as expressed by the unresolved product in Eq. 26.

However, we are faced with a substantial question by considering Eq. 31. Is there any similarity with the concept of inertial speed? We believe the answer is somehow yes, but first we should consider the great difference between both concepts. Inertial speed²⁶ refers to the exposure axis on a logarithmical scale, whereas the polynomial coefficient correlates strikingly with the photon absorption rate because of its dependence on the square of the limit value x_{1L} . Accordingly, b_2 changes drastically with A_1 , quite in corresponding contrast to the rather constant behavior of the *inertial speed* as designated by the formulation of the adjective *inertial* itself.

But nevertheless, both concepts relate to the sensitivity in the beginning range of a photographic characteristic curve. In this context, we have found an interesting correlation if the development conditions are changed. The details are provided later in this article.

3. More specified information provides the limit value x_{3L} . We may derive this result from the polynomial coefficient given before by using Eq. 38. Via this value, we get the quotient between the limit value x_{2L} for silver cluster nucleation and the retardation parameter C_2 for silver cluster growth. In other words, the efficiency of the former process is related to the inefficiency of the latter, because of dispersity and other effects. However, it may be believed that the limit value x_{3L} reflects changes of the nucleation speed preferably in systematic studies where the photon absorption rate is changed. Dispersity effects that

influence silver cluster growth should not be changed very significantly for the moderate exposure conditions as applied in our studies.

4. More profound analysis provides the identification of the limit value x_{2L} itself. From the dependence on the limit value x_{1L} , we obtain access to both driving parameters of silver cluster nucleation speed, i.e., to both parameters B_1 and B_2 , made available with the help of Eq. 13.

However, from Eq. 26 we obtain the undissolved product $a_2 a_3$ only and not the value of a_2 alone. To solve the problem, we may refer to a method published elsewhere.¹³ Thus, it appears convenient to approximate the parameter a_2 by a reasonably low value, if the photon absorption rate is not very great as well, e.g., by $a_2 = 4000$ related to $K = 1000$. This allows us to unveil the parameter a_3 , and also the value of C_1 by using the corresponding expression $a_3 = C_1 \cdot x_{1L}$ from Eqs. 21 and 26, respectively. The identified value of C_1 may then be applied properly for other exposure ranges as well to decompose the product above.

We believe that both parameters B_1 and B_2 are bound preferably to the activation of the mobile Ag^+ ion system as required for silver cluster nucleation in subimage formation. But, different mechanisms for photoelectron transfer should be reflected as well. Thus, the first process is assumed to proceed preferably via a conduction band mechanism, while the second may be bound to some trapped-state dynamics for providing a higher order mechanism in dependence on the photoelectron density.

5. A very instructive result is the limit value x_{1L} . We get a photophysically well-defined quantity that correlates directly with the photoelectron excitation characteristics. The value may be used to determine the photoelectron lifetime τ . This access is unique in comparison with direct measurements, where strong excitation is required that deviates strikingly from image like exposure. By way of our determination, we may proceed to very sophisticated studies of realistic emulsions to elucidate the dependence on smooth changes of a number of correlated influences such as the photon absorption rate and the wavelength of monochromatic radiation during exposure. Both photoelectron excitation and silver clustering become clearly discriminated from each other. But they may be observed simultaneously with good resolution as well.

Analysis of LIRF. This effect has been well established in all photomaterials studied so far, i.e., in diagnostic x-ray films from different producers.^{11,13-17} From monochromatic time-scale sensitometry, we always found a significant LIRF if the photon absorption rate has been systematically diminished by 1 to 3 orders of magnitude.

The mechanism is largely independent of the primary way of photoexcitation, which has been changed from intrinsic AgX lattice absorption to sensitizing dye absorption by varying the exposure wavelength from 425 to 550 nm, respectively. There was never a serious influence on the photoelectron lifetime dependent on both the spectral change before and the photon absorption rate. But we found a steep correlation between both limit values x_{1L} and x_{2L} , in accordance with Eq. 13.

Thus, the LIRF could be attributed to the changing efficiency of the silver cluster nucleation process owing to a strong influence of the nonlinear term as expressed by the product $B_2 x_{1L}^2$ in Eq. 2. The unveiled mechanism is in

good agreement with previous explanations of LIRF as made by other authors on the basis of the thermodynamic phase-building theory,²³ for example.

By comparing photomaterials from different producers, some changes could be unveiled in a quantitative sense only, i.e., higher photoelectron lifetimes might correlate with lower limit values x_{2L} , and vice versa. This reflects some peculiarities between the ripening states that deserve further attention by more directed studies.

The results above differ from those of corresponding studies with monochromatic exposure lower than 400 nm, which will be discussed more below.

Influence of Development. Changing development conditions provide substantial proof of our methodology. AgX photophysics do not depend on a subsequent step. This must be properly reflected by our analysis as well.

Below we refer to results as published elsewhere.¹⁴ The proof has been carried out by a cross experiment. Both the development and the photon absorption rate have been varied between two distinct regimes.

Accordingly, diagnostic x-ray film HS 90 has been exposed with monochromatic radiation at 425 nm for two different photon absorption rates varying by 3 orders of magnitude. Then, development has been carried out either in a standard way (i.e., T 30) used normally to obtain maximum speed for diagnostic application or with a second procedure (i.e., R09) on the basis of para-aminophenol. The second procedure is well-known for achieving rather equilibrated gradations.

Standard development provides higher speed, but not in every case. The difference was restricted to the higher photon absorption rate only. This has been reflected by the limit values x_{1L} , while the limit value x_{3L} , has been left almost unchanged.

The results exclude any change of the so-called development criterion between both regimes that refers to a different critical size of the latent image center for catalyzing development. But the influence on the limit value x_{1L} may be interpreted quite properly by considering a topological effect that occurs in light-exposed AgX microcrystals. Thus, photoelectrons shift increasingly into the subsurface region if the photon absorption rate is raised, and latent image formation will be shifted too. In this case, the centers may be made available by standard development because of the high sulphite content, but not by surface development with R09.

In this last context, we refer to the concept of inertial speed once more. The method applies to density-scale sensitometry. But the analysis is restricted to the beginning of the curve where the photon absorption rate may be assumed as rather small. The topological shift should not yet play a significant role. Thus, the inertial speed too might be basically independent of corresponding changes of the development regime, which is quite in accord with previous statements made many decades ago.

Spectral Dependence in Extended Studies. Both studies provide an important conclusion. The usual understanding of photographic behavior was basically confirmed, and the method may be considered as well proved. Thus, we may start on further investigation of more substantial aspects.

Below we extend the measurement to higher quantum energies beneath 400 nm. This spectral range is assumed to be a turning point for AgX photophysics according to Mitchell.¹ Direct photolysis of the AgX lattice should be

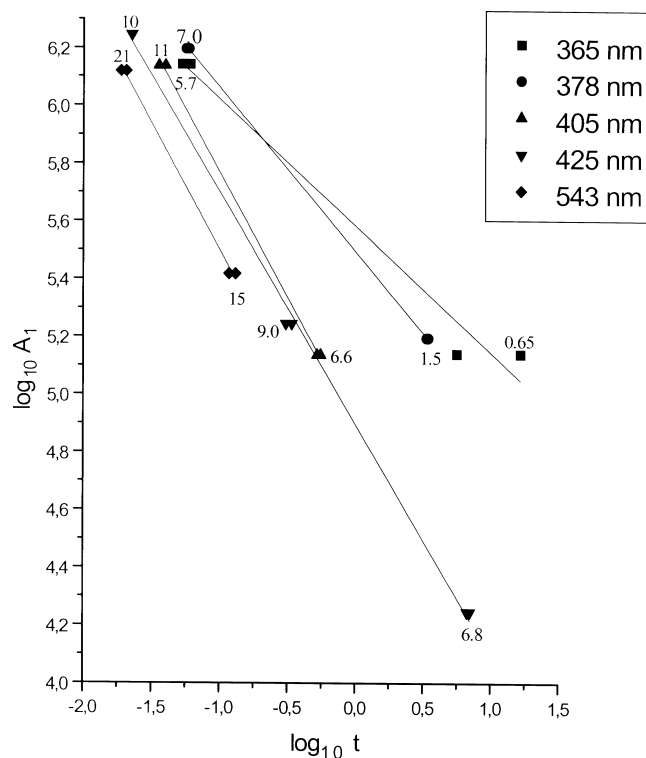


Figure 3. Equidensities as derived from monochromatic time-scale sensitometry for the same photomaterial as used in Fig. 2. The wavelength has been varied above and below the 400 nm range. All curves relate to the Burton-Berg corrected density of 0.5. At the ordinate, the photon absorption rate A_1 are designated as absolute values on a logarithmic scale. The numbers at the single points within the graph indicate the photoelectron lifetime in microseconds.

excluded for absorbed photons with lower quantum energies (i.e., for wavelengths beyond 400 nm), because of the first law of thermodynamics. Mitchell discusses an Auger decay of excitons at so-called donor centers. They should be involved actively within the primary process of photoexcitation to overcome the energy deficit.

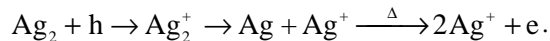
The Auger decay should lead to the creation of photoelectrons, but not of holes normally. This is in contrast to the concept of pair generation of photoelectrons and holes as assumed generally by the direct photolysis theory of latent image formation, according to Gurney and Mott. Mitchell allows such a possibility for spectral ranges with higher quantum energies only, i.e., for wavelengths below 400 nm.¹

The results of our investigation are depicted in Fig. 3. The equidensities have been derived from monochromatic time-scale sensitometry above and below 400 nm. The crucial point of the proof is the reliability of the photon absorption rate as indicated on logarithmic scale at the ordinate. Meticulous measurements were performed with different methods (by using a photodiode and a thermopile head) to exclude deficient calibration of the radiometer for the varying spectral ranges studied.

We obtained unique hints of drastic changes of the elementary process by crossing the 400-nm range. On a macroscopic scale, we obtained a drop in quantum sensitivity, i.e., the sensitivity was somewhat less at below 400 nm compared to above. But the major effects were found on a microscopic scale. For higher quantum energies, we observed an expressed dependence of the photoelectron lifetime on the photon absorption rate. This differs strikingly from the

rather uniform behavior as found for lower quantum energies above the 400 nm range.

The results may be well understood within the framework of the photoaggregation theory as expressed by Mitchell.¹ The lack of holes should be reflected quite properly by the uniform behavior of the photoelectron lifetime as observed for the range of lower quantum energies (i.e., beyond 400 nm). In a similar way, the appearance of holes should be reflected as well, i.e., by the increase of the photoelectron lifetime in dependence on the photon absorption rate as observed for higher quantum energies at lower than 400 nm. This may be explained by assuming a hole attack at donor centers that would open an additional pathway for photoelectron generation according to



The last step is a thermally activated one. It is likely, that the decay probability correlates with thermal energy dissipation in dependence on the photon absorption rate.

Conclusion and Outlook

It may be concluded that the methodology offers great future prospects. Clustering rate analysis is a promising method to unveil microscopic information from properly controlled time-scale sensitometry. The approach is unique for adequate studies of latent image formation under relevant conditions of camera-sensitive exposure and with realistic photomaterials.

The method has stood the test with respect to different criteria. The uniqueness of parameter identification could be established, and the interpretation was always in accord with the usual understanding of major effects in photographic behavior studied so far. Thus, a basic problem has been adequately solved, i.e., the use of dynamical concepts of systems analysis to describe latent image formation in some aggregated way that remains flexible enough to analyze relevant photophysics properly as reflected in sensitometric curves.

The subsequent disaggregation of the macroscopic response provides an outstanding tool. We obtain insight into a series of hierarchically ordered subsystems as determined by photoelectronic and ionic processes in combination with silver cluster nucleation and growth. Mechanistic conclusions should be consolidated more properly in this way than by ingenious reconstruction from single process investigations performed under differently specified conditions.

The method seems capable of resolving substantial questions of latent image theory by proper combination of results from meticulous studies provided the exposure and development conditions are varied systematically. Our analyses very strikingly support some arguments as expressed by the photoaggregation theory of Mitchell.¹ The corresponding conclusions have been drawn from the determination of the photoelectron lifetime in dependence on both the spectral range and the photon absorption rate. The wavelength range of 400 nm could be established as a threshold for primary photoexcitation quite in accord with the predictions of Mitchell.

The methodology remains open to further sophistication and improvement in extended studies. Of great future interest should be the ingenious combination of simulation methods acting on differing principles by a top-down and a bottom-up approach. But this requires the precise fitting of sensitometric data for all methods that have to be compared. Relevant studies are planned for the future. ▲

Acknowledgments. The authors are deeply indebted to Prof. Manfred Peschel and Wolfgang Schirmer for many helpful discussions and inspiring comments throughout this work and for carefully reading the manuscript.

Great thanks are expressed also to Dr. H. Zwicky, Dr. W. Spahni, and DC G. Wendler from Typon AG für Photographische Industrie in Burgdorf, Switzerland, for interesting discussions and for kindly providing us with the photomaterials studied.

References

1. J. W. Mitchell, The basic concepts of photoaggregation theory, *J. Imag. Sci. Technol.* **39**, 193 (1995).
2. G.P. Nutting, On the absorption of light in heterogeneous media, *Phil. Mag.* **26**, (1913).
3. C. E. K. Mees, in *The Theory of the Photographic Process*, The Macmillan Company, New York, 1954, p. 106.
4. P. C. Burton and W. F. Berg, *Phot. J.* **86B** (2).
5. B.E. Bayer and J.F. Hamilton, Computer investigation of a latent image model, *J. Opt. Soc. Am.* **55**, 439 (1964).
6. E. Gerth, Zur analytischen darstellung der schwärzungskurve I, *Z. Wiss. Phot.* **60**, 106 (1967).
7. E. Gerth, Reaktionskinetische betrachtungen zur entstehung des-latenten bildes und der photographischen schwärzung I, *Bild und Ton* **26**, 45 (1973).
8. *Ibid.* II **26**, 69 (1973).
9. *Ibid.* III **26**, 107 (1973).
10. E. Gerth, On the analytical treatment of blackening curves. III. The reaction tensors of photographic process, *J. Inf. Rec. Materials* **6**, 421 (1978).
11. L. Dünkel, M. Peschel and E. Nutsch, A new systems-analytical approach to the study of the photographic process, *Syst. Anal. Model. Simul.* **6**, 109 (1989).
12. L. Dünkel and E. Nutsch, Mathematical modeling, simulations and analysis of the dynamical properties of the photographic process. part 1: solutions of the hierarchically coupled driving-force model (HCD model) by closed integration, *Cybernet. Syst. Int. J.* **23**, 105 (1992).
13. L. Dünkel, E. Nutsch, and B. Kutschan, Mathematical modeling, simulations and analysis of the dynamical properties of the photographic process. part 2: systematics of parameter identification in the application of the hierarchically coupled driving-force model (hcd model) by the study of light-induced processes in photographic materials, *Cybernet. Syst. Int. J.* **24**, 281 (1993).
14. L. Dünkel, E. Nutsch and B. Kutschan, The HCD model approach to a process-correlated sensitometry in photographic science. part 3: special studies for revealing the influence of different development conditions on the result of parameter identification and their physical interpretation, *Proc. Cybernetics Syst. '94, 12th European Meeting on Cybernetics and Systems Research*, University of Vienna 5–8 April, 1994, p. 119.
15. L. Dünkel, E. Nutsch and B. Kutschan, The photographic elementary process in mechanistic studies with the help of the HCD model, *Proc. IS&T's 47 Annual Conference/ICPS 1994*, p. 294.
16. L. Dünkel, E. Nutsch and B. Kutschan, The spectral dependence of the lifetime determination for photoelectrons derived from clustering rate analysis by HCD model studies, *Proc. IS&T's 48th Annual Conference*, 1995, p. 328.
17. L. Dünkel, E. Nutsch and B. Kutschan, Decision-making based on HCD model studies of the photographic response, *Proc. IS&T's 48th Annual Conference*, 1996, p. 80.
18. J. C. Dainty and R. Shaw, *Image Science Principles, Analysis and Evaluation of Photographic-Type Imaging Processes*, Academic Press, San Francisco, 1974, p. 1.
19. T. Svedberg, On the reaction between sensitiveness and size of grain in photographic emulsions part II, *Phot. J.*, **62**, 186 (1922).
20. M. Peschel and W. Mende, The predator prey model: Do we live in a volterra world? Springer-Verlag, Berlin, 1986, p. 53.
21. A. N. Tichonov, *Mat. Sbornik* **31**, 575 (1952).
22. R. H. Bube, *Photoelectronic Properties of Semiconductors*, Cambridge University Press, 1992, p. 1.
23. E. Moisar, F. Granzler, D. Dautrich and E. Palm, Formation and properties of sub-image and latent image silver specks—A process of nucleation and phase formation, *J. Photogr. Sci.*, **28**, 71 (1982).
24. I. N. Bronstein, K. A. Semendjajew, G. Musiol, and H. Mühlhig, *Taschenbuch der Mathematik*, Verlag Harry Deutsch Thun und Frankfurt am Main, 1995, p. 380.
25. *Ibid.* p. 285.
26. C. E. K. Mees, *The Theory of the Photographic Process*, The Macmillan Company, New York, 1954, p. 226.
27. W. Ebeling and R. Feistel, *Physik der Selbstorganisation und Evolution*, Akademie Verlag Berlin, 1982, p. 224.
28. C. W. Gardiner, *Handbook of Stochastic Methods*, 2nd ed., Springer-Verlag, Berlin, 1985, p. 197.